Progress In Electromagnetics Research, *PIER 31, 225–245, 2001*

BISTATIC SCATTERING AND BACKSCATTERING OF ELECTROMAGNETIC WAVES BY CONDUCTING AND COATED DIELECTRIC SPHEROIDS: A NEW ANALYSIS USING MATHEMATICA PACKAGE

L.-W. Li, T.-S. Yeo, and M.-S. Leong

Department of Electrical & Computer Engineering
The National University of Singapore
10 Kent Ridge Crescent, Singapore 119260

Abstract–Solutions to electromagnetic scattering at any angle of incidence by a perfectly conducting spheroid and a homogeneous dielectric spheroid coated with a dielectric layer are obtained by solving Maxwell's equations together with boundary conditions. The method used is that of expanding electric and magnetic fields in the spheroidal coordinates in terms of the spheroidal vector wave functions and matching their respective boundary conditions at spheroidal interfaces. In this formulation, the column vector of the series expansion coefficients of the scattered field is obtained from that of the incident field by means of a matrix transformation, which is in turn obtained from a system of equations derived from boundary conditions. The matrix depends only on the scatterer's properties; hence the scattered field at a different direction of incidence is obtained without repeatedly solving a new set of simultaneous equations. Different from the previous work, the present work developed an accurate and efficient Mathematica source code for more accurate solution to the problem. Normalized bistatic and backscattering cross sections are obtained for conducting (for verification purpose), homogeneous dielectric (for verification purpose), and coated dielectric prolate (for some new results) spheroids, with real and complex permittivities. Numerically exact results for the coated dielectric prolate spheroids are newly obtained and are not found in existing literature.

1. INTRODUCTION

There has always been an interest in the study of electromagnetic scattering by various objects, whether it be the conducting type or the dielectric type. Such solutions play an important role in the computation of scattering cross sections of these objects and their characteristics of radar objects. Aside from providing exact solutions for the respective geometries, they are invaluable in the evaluation of approximate and numerical solutions. Over many years, electromagnetic scattering by spheroidal objects has been a hot topic in scientific research and engineering application. This is not surprising, since the exact or analytic solutions to such scattering by their spherical and cylindrical cousins are quite abundant in the literature [1–5].

In the past half a century, one of the first numerical results on electromagnetic scattering from prolate conducting spheroids for axial incidence was given by Siegel *et al.* [6] for spheroids with a major to minor axial ratio of 10. This was later improved by Sinha and MacPhie [7] who also provided some new results for axial ratios different from 10. Sinha and MacPhie later also came up with the backscattering cross sections of conducting prolate spheroids [8] for any arbitrary angle of polarization. In all these works, the approach used was an analytic one which involves expansions of the electromagnetic fields in terms of prolate spheroidal vector wave functions [9], and matching for of boundary conditions.

The solution in the dielectric case was first given by Asano and

Yamamoto [10]. They also used the same analytic approach in their investigation of light scattering from spheroidal particles. They produced the bistatic and backscatter cross sections for a wide variety of spheroids of different materials and dimensions. In a similar way, the results for a dielectric spheroid coated with another dielectric layer were produced by Cooray and Ciric [11]. Coated spheroids have also been considered by Peterson [12] and Wang [13] where the extended boundary conditions (T-matrix) method was applied. The results were obtained basically for small atmospheric and biological particles.

The objective of this paper is to revisit the electromagnetic scattering from conducting and dielectric spheroids using a *Mathematica* package and to obtain some new results of bistatic and backscatter cross sections for the latter case and some more accurate results for the former cases. This is possible through the work of Li *et al.* [14], who came up with the *Mathematica* packages for the spheroidal angular and radial functions, both of which form the basis of the spheroidal vector wave functions. As claimed by Li *et al.* [14], the package is accurate to any useful significant digits of solutions, valid for both real and complex arguments of spheroidal angular and radial functions, and accurate for any large argument of the eigenvalue problem and spheroidal vector wave functions. In this connection, the analysis is of very high accuracy although the approach used is still that of Sinha [8], i.e., an exact solution is obtained by expanding the incident and scattered fields in terms of prolate spheroidal vector wave functions [9] but computed numerically for various cases. Results of the bistatic and backscattering cross sections computed for spheroids of different dimensions and materials and different angles of incidence are presented in this paper. A comparison of computed data for a few cases with those results available in the literature is made to demonstrate show that the high accuracy of the present solutions.

2. SPHEROIDAL WAVE FUNCTIONS AND THEIR COMPUTATIONS

2.1 Spheroidal Coordinates System

The spheroidal coordinates [9, 14, 15] are obtained by the rotation of an ellipse about an axis of symmetry. Two cases are to be distinguished, according to whether the rotation takes place about the major axis (prolate spheroid) or about the minor axis (oblate spheroid). It

is customary to make the z-axis to be the axis of revolution in each case. The semifocal distance is usually denoted by F.

The two coordinates systems $(\eta,\ \xi,\ \phi)$, where η is an angular coordinate, ξ is a radial one, and ϕ is an azimuthal one, are related to the Cartesian system $(x,\ y,\ z)$ by the transformation

$$x = F(1-\eta^2)^{1/2}(\xi^2 \mp 1)^{1/2}\cos\phi, \tag{1a}$$

$$y = F(1-\eta^2)^{1/2}(\xi^2 \mp 1)^{1/2}\sin\phi, \tag{1b}$$

$$z = F\eta\xi, \tag{1c}$$

with $-1 \le \eta \le 1,\ 1 \le \xi < \infty$, and $0 \le \phi \le 2\pi$ for the prolate system and with $-1 \le \eta \le 1,\ 0 \le \xi < \infty$, and $0 \le \phi \le 2\pi$ for the oblate one. In both pairs of signs in the inequalities above and in the expressions that follow, the upper sign corresponds to the prolate spheroidal system and the lower one to the oblate system in (1).

2.2 Spheroidal Radial and Angular Functions

In following Flammer's notation, we set $d = 2F$ and $c = kd/2$. Solutions of the scalar wave equation in the prolate spheroidal coordinates

$$(\nabla^2 + k^2)\psi = 0 \tag{2}$$

are obtainable using separation of variables [9]. It results in the solution of

$$\psi_{\substack{e\\o}mn} = S_{mn}(c,\eta)R_{mn}(c,\xi)\begin{matrix}\cos\\ \sin\end{matrix} m\phi \tag{3}$$

where $R_{mn}(c,\ \xi)$ and $S_{mn}(c,\ \eta)$ are the spheroidal radial and angular functions, respectively. The subscripts e and o denote even and odd ϕ-dependences of functions, respectively.

The angular functions can be expressed as an infinite series of the associated Legendre functions of the first kind as

$$S_{mn}(c,\eta) = \sum_{r=0,1}^{\infty}{}' d_r^{mn}(c)P_{m+r}^m(\eta), \tag{4}$$

where the $d_r^{mn}(c)$ denotes the expansion coefficients given by Flammer [9], and the prime over the summation symbol indicates that the summation is over even values of r only when $(n-m)$ is even and over

odd values of r only when $(n-m)$ is odd. Thus, the spheroidal angular functions depend not only on the angular component, but also on the characteristics of the medium and the size of the spheroid through the parameter c. Flammer [9] also derived an alternative form of expression for the angular functions which allows us to deduce certain properties: $S_{mn}(\eta)$ is zero when $\eta = 1$ for all values of m except for $m = 0$. When $\eta = 0$, $S_{mn}(\eta) = 0$ for odd values of $(n - m)$.

The radial functions $R_{mn}(c,\ \xi)$ can be expressed in terms of the spherical Bessel functions [9] as

$$R_{mn}^{(j)}(c,\xi) = \left[\sum_{r=0,1}^{\infty}{}' \frac{(2m+r)!}{r!} d_r^{mn}(c)\right]^{-1} \left(1 - \frac{1}{\xi^2}\right)^{m/2} \cdot \sum_{r=0,1}^{\infty}{}' i^{r+n-m} \frac{(2m+r)!}{r!} d_r^{mn}(c) Z_{m+r}^{(j)}(c\xi) \tag{5}$$

in the prolate case, where $Z_n^{(j)}(c\xi)$ is the nth-order spherical Bessel, Neumann, and Hankel functions of the first and second kinds in order of $j = 1,\ 2,\ 3$, and 4, respectively, and d_r^{mn} are the same expansion coefficients as in Eq. (4). The first order derivatives these functions are obtained by differentiating Eq. (5) directly.

The spherical Bessel functions are regular in every finite domain of the $c\xi$ plane, including $c\xi = 0$, whereas the spherical Neumann functions have singularities at the origin $c\xi = 0$ and in fact they become infinite. We shall, therefore, use the radial functions $R_{mn}^{(1)}$ instead of $R_{mn}^{(2)}$ to represent the waves inside the spheroid and the incident wave. At very large distances from the spheroid, on the other hand, the scattered wave approaches a spherical diverging wave with centre of the spheroid as its centre. From the asymptotic behaviour given above, the third and fourth kinds of radial functions, $R_{mn}^{(3)}$ and $R_{mn}^{(4)}$, would be suitable to represent the scattered waves.

The solution of the vector wave equations in the spheroidal coordinates can be formed in terms of a set of vector wave functions, $\boldsymbol{M}$ and $\boldsymbol{N}$, analogous to those developed for the sphere [1]

$$\boldsymbol{M}_{\substack{e\\o}mn}^{q(p)}(\eta,\xi,\phi) = \nabla\psi_{\substack{e\\o}mn}^{(p)}(\eta,\xi,\phi) \times \widehat{\boldsymbol{q}}, \tag{6}$$

$$\boldsymbol{N}_{\substack{e\\o}mn}^{q(p)}(\eta,\xi,\phi) = \frac{1}{k}\nabla \times \boldsymbol{M}_{\substack{e\\o}mn}^{q(p)}(\eta,\xi,\phi) \tag{7}$$

where k denotes the wavenumber of the incident wave, $\widehat{\boldsymbol{q}}$ stands for an arbitrary constant vector ($\widehat{\boldsymbol{q}} = \widehat{\boldsymbol{x}}$, $\widehat{\boldsymbol{y}}$ or $\widehat{\boldsymbol{z}}$), or the position vector $\widehat{\boldsymbol{r}}$, p represents the kind of the radial function involved, and $\psi(\eta, \xi, \phi)$ is given by (3).

3. ELECTROMAGNETIC SCATTERING BY A CONDUCTING SPHEROID

We shall first consider the scattering of a plane, linearly polarized monochromatic wave by a perfectly conducting spheroid immersed in a homogeneous, isotropic medium. It is assumed that the surrounding medium is non-conducting and non-magnetic. Results are only presented for the prolate spheroids, as the results for the oblate cases can be obtained by the transformations $\xi \to i\xi$ and $c \to -ic$.

3.1 Spheroidal Geometry

The semimajor and semiminor axes of the spheroid are denoted by a and b respectively. These are related to the parameter ξ via:

$$2a = d\xi, \tag{8a}$$

$$2b = d(\xi^2 - 1)^{1/2}, \tag{8b}$$

and the surface of the spheroid is given by

$$\xi_0 = \frac{a}{(a^2 - b^2)^{1/2}} = \frac{a/b}{[(a/b)^2 - 1]^{1/2}}. \tag{9}$$

Similarly, the parameter, c, can be obtained using (8a):

$$c = \frac{1}{2}kd = \frac{ka}{\xi}. \tag{10}$$

The geometry of the configuration is as shown in Fig. 1.

3.2 The Incident and Scattered Fields

Without loss of generality, the direction of propagation of the linearly polarized monochromatic incident wave is assumed to be in the x-z plane, making an angle θ_0 with the z-axis, as shown in Fig. 1. The time dependence, $\exp(-jwt)$, is assumed and suppressed throughout.

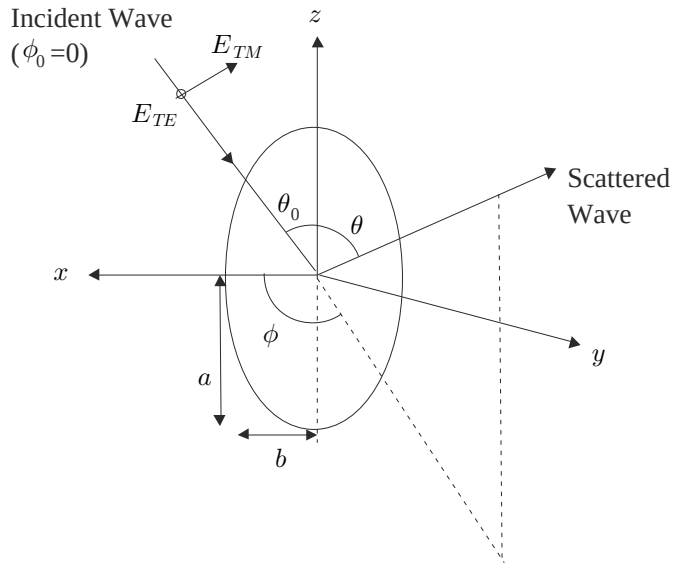

Figure 1. Scattering geometry for a prolate spheroid.

For oblique incidence ($\theta_0 \neq 0$), the polarized incident wave is resolved into two components: the TE mode for which the electric vector of the incident wave vibrates perpendicularly to the $x-z$ plane, and the TM mode in which the electric vector lies in the $x-z$ plane. Thus the plane wave expressions for both modes are given by

$$\boldsymbol{E}_{TE} = E_{TEO}\widehat{\boldsymbol{y}}e^{-j\boldsymbol{k}.\boldsymbol{r}}, \tag{11}$$

$$\boldsymbol{E}_{TM} = E_{TMO}(-\widehat{\boldsymbol{x}}\cos\theta_0 + \widehat{\boldsymbol{z}}\sin\theta_0)e^{-j\boldsymbol{k}.\boldsymbol{r}} \tag{12}$$

where E_{TEO} and E_{TMO} are the amplitudes of the TE and TM fields respectively, and

$$-\boldsymbol{k}.\boldsymbol{r} = k(x\sin\theta_0 + z\cos\theta_0) \tag{13}$$

with k as the wave number of the monochromatic radiation.

The incident wave excited can be described in terms of vector wave functions [9] as follows:

$$\boldsymbol{E}_{TE} = \frac{E_{TEO}}{k\cos\theta_0}\sum_{m=0}^{\infty}\sum_{n=m}^{\infty}A_{mn}(\theta_0)\boldsymbol{M}_{emn}^{x(1)}(\eta,\xi,\phi), \tag{14}$$

$$\boldsymbol{E}_{TM} = \frac{E_{TMO}}{k}\sum_{m=0}^{\infty}\sum_{n=m}^{\infty}A_{mn}(\theta_0)\boldsymbol{M}_{emn}^{y(1)}(\eta,\xi,\phi), \tag{15}$$

where the expansion coefficient is expressed as

$$A_{mn}(\theta_0) = \frac{2\epsilon_m j^{n-1}}{N_{mn}} S_{mn}(\cos\theta_0) \tag{16}$$

and the $\boldsymbol{M}$ vectors are those given in Eq. (6). Note that the radial functions of the first kind are used for the incident wave because they are finite at the coordinate origin, as mentioned previously.

For axial incidence (at $\theta_0 = 0$), there is no need to consider two modes by virtue of symmetry. The wave is then assumed to be propagating along the negative z-axis with its electric field polarized along the positive y-axis and magnetic field along the positive x-axis. However, if $\theta_0 = 0$, then $\cos(\theta_0) = 1$ and $S_{mn}(1) = 0$ for all $m > 0$. In other words, by Eq. (16), A_{mn} is non-zero only for $m = 0$ and the expansions is thus defined only for $m = 0$ at axial incidence:

$$\boldsymbol{E}_i = \frac{E_i}{k} \sum_{n=0}^{\infty} A_{0n}(0) \boldsymbol{M}_{e0n}^{x(1)}(\eta, \xi, \phi), \tag{17a}$$

$$A_{0n}(0) = \frac{2j^{n-1}}{N_{0n}} S_{0n}(1). \tag{17b}$$

To describe the scattered fields, we can use the radial functions of the fourth kind in the case of the present time dependence because the Sommerfeld radiation condition must be satisfied. The radial functions of the fourth kind are suitable because of their asymptotic behaviours. This ensures that at large distances from the spheroid, the scattered wave behaves as a spherical diverging wave, emanating from the spheroid center. The components of the scattered field must also have the same ϕ-dependence as the corresponding components of the incident field (ϕ-matching).

To satisfy these requirements, we can write

$$\boldsymbol{E}_{STE} = \sum_{m=0}^{\infty} \sum_{n=m}^{\infty} \left(\alpha_{mn} \boldsymbol{M}_{e,m+1,n}^{+(4)} + \gamma_{mn} \boldsymbol{M}_{emn}^{z(4)} \right), \tag{18}$$

$$\boldsymbol{E}_{STM} = \sum_{m=0}^{\infty} \sum_{n=m}^{\infty} \left(\beta_{mn} \boldsymbol{M}_{o,m+1,n}^{+(4)} + \rho_{m+1,n+1} \boldsymbol{M}_{o,m+1,n+1}^{z(4)} \right) + \sum_{n=1}^{\infty} \beta_{1n}^{-} \boldsymbol{M}_{o1n}^{-(4)} \tag{19}$$

where $\boldsymbol{E}_{STE}$ and $\boldsymbol{E}_{STM}$ are respectively the scattered fields corresponding to the TE and TM incident fields and α_{mn}, γ_{mn}, β_{mn},

$\rho_{m+1,n+1}$ are the unknown expansion coefficients to be determined using boundary conditions. An extra term is needed at the end of Eq. (19) due to the nature of the ϕ-dependence of the odd vector wave functions.

3.3 Transformation of Incident Fields to Scattered Fields

Assuming the prolate spheroid to be perfectly conducting, the incident field $\boldsymbol{E}$ and the scattered field $\boldsymbol{E}_s$ must satisfy the boundary conditions at $\xi = \xi_0$:

$$E_\eta + E_{s\eta} = 0, \tag{20a}$$

$$E_\phi + E_{s\phi} = 0, \tag{20b}$$

where the suffixes η and ϕ denote respectively the η- and ϕ-components of the incident and scattered fields. Eq. (20) must hold for all allowed values of $0 \le \phi \le 2\pi$ and $-1 \le \eta \le 1$. In the similar fasion, boundary conditions satisfied by the magnetic field components can also be applied to obtain the coefficients.

The series coefficients of the scattered field are then obtained from the series coefficients of the incident field by means of a matrix transformation, i.e.,

$$\boldsymbol{S} = [G]\boldsymbol{I}. \tag{21}$$

The novelty of this approach is that the matrix $[G]$ depends only on the scatterer's properties. Given any spheroidal body, the scattered coefficient column vector $\boldsymbol{S}$ can be obtained easily from the incident coefficient column vector $\boldsymbol{I}$ using the same equation, regardless of the angle of incidence or the nature of principal polarization. There is no need to find another matrix for a new angle of incidence, and much work is thus saved in the process. Moreover, the matrix used for the TE polarization can be used to derive the matrix for the TM case without any extra effort.

To obtain the matrix, we substitute the field expressions into the above equations and expand them in terms of the vector wave functions. We then make use of the orthogonality of the trigonometric functions by multiplying throughout by $\sin(m+1)\phi$ or $\cos(m+1)\phi$ where $m \ge 0$, and then by integrating them with respect to ϕ from 0 to π. Next, to remove the η-dependence of the equations, we make use of the orthogonal properties of the spheroidal angular functions. This is done by multiplying both sides of each equation by $S_{m,m+N}$ where

$N = 0, 1, 2, \ldots$, and then by integrating both sides over the complete range of $\eta \in (-1 \leq \eta \leq 1)$. Finally, we are left with an infinite system of equations satisfied by an infinite set of unknown scattering coefficients, with one equation for each m. To obtain numerical results using the computer, the system has to be truncated to a finite number of equations satisfied by the same number of unknowns according to uniqueness of the solution. In this paper, the truncation number m_t for m (i.e., $m = 0, 1, 2, \cdots, m_t - 1$) and the truncation number n_t for n belonging to each m (i.e., $n = m, m+1, \cdots, m+n_t-1$) were each taken to be `Integer(ka+4)`. This is the scheme suggested by Sinha and MacPhie [7, 8] and is followed herein.

3.4 Far Field Expressions

Using Eqs. (18) and (19) and far-field conditions, we get the following normalized bistatic cross sections at non-axial incidence:

$$\frac{\pi\sigma(\theta,\phi)}{\lambda^2} = |F_\theta(\theta,\phi)|^2 + |F_\phi(\theta,\phi)|^2, \tag{22}$$

where

$$F_\theta(\theta,\phi) = \sum_{m=0}^{\infty}\sum_{n=m}^{\infty} -\frac{j^n}{2}\alpha'_{mn} S_{mn}(\cos\theta).\sin(m+1)\phi, \tag{23}$$

$$F_\phi(\theta,\phi) = \sum_{m=0}^{\infty}\sum_{n=m}^{\infty} j^n \left[\frac{\alpha'_{mn}}{2}\cos\theta S_{mn}(\cos\theta) - j\gamma'_{m+1,n+1}\sin\theta S_{m+1,n+1} \cdot (\cos\theta)\right] \cdot \cos(m+1)\phi - \sum_{n=0}^{\infty} j^n \gamma'_{0n}\sin\theta S_{0n}(\cos\theta), \tag{24}$$

for TE polarization; and

$$F_\theta(\theta,\phi) = \sum_{m=0}^{\infty}\sum_{n=m}^{\infty} \frac{j^n}{2}\beta'_{mn} S_{mn}(\cos\theta).\cos(m+1)\phi - \sum_{n=1}^{\infty} j^n \frac{\beta^{-\prime}_{1n}}{2} S_{1n}(\cos\theta), \tag{25}$$

$$F_\phi(\theta,\phi) = \sum_{m=0}^{\infty}\sum_{n=m}^{\infty} j^n \left[\frac{\beta'_{mn}}{2}\cos\theta S_{mn}(\cos\theta) - j\rho'_{m+1,n+1}\sin\theta S_{m+1,n+1}(\cos\theta)\right]\sin(m+1)\phi, \tag{26}$$

for TM polarization.

When $\theta = \theta_0$ and $\phi = 0$, we obtain the normalized backscattering cross section

$$\frac{\pi\sigma(\theta_0)}{\lambda^2} = |F_\theta(\theta_0, 0)|^2 + |F_\phi(\theta_0, 0)|^2, \tag{27}$$

for different values of the incident angle θ_0.

4. ELECTROMAGNETIC SCATTERING BY A COATED DIELECTRIC SPHEROID

4.1 Spheroidal Geometry

In this section, we consider a dielectric spheroid coated by dielectric material. Both the medium in spheroid and its coating layer are assumed to be linear, homogeneous, isotropic, and non-magnetic in nature, but with different permittivities ϵ_1 and ϵ_2 (in general complex quantities), respectively. The geometry of this problem is shown in Fig. 2

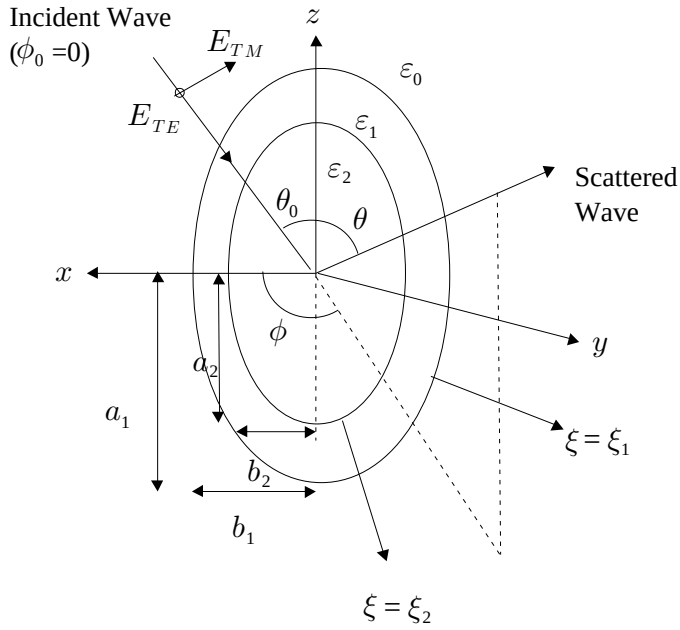

Figure 2. Scattering geometry for a coated dielectric spheroid.

The relationships governing the parameters c and ξ, and the spheroidal dimensions are the same as those in the previous section. In addition, the following holds :

$$\frac{\xi_1}{\xi_2} = \frac{a_1}{a_2}, \tag{28}$$

$$c_1 = \sqrt{\frac{\epsilon_1}{\epsilon_0}} c_0, \tag{29}$$

$$c_2 = \sqrt{\frac{\epsilon_2}{\epsilon_0}} c_0. \tag{30}$$

4.2 The Incident, Transmitted and Scattered Fields

The incident and scattered electric fields for TE and TM polarizations are the same as those in Eqs. (14), (15), (18), and (19) of the conductor case. The transmitted fields inside the core ($\xi < \xi_2$) can be expressed as

$$\boldsymbol{E}^2_{t,TE} = \sum_{m=0}^{\infty} \sum_{n=m}^{\infty} \left(\sigma^E_{mn} \boldsymbol{M}^{+(1)}_{e,m+1,n}(c_2) + \tau^E_{mn} \boldsymbol{M}^{z(1)}_{emn}(c_2) \right), \tag{31a}$$

$$\begin{aligned} \boldsymbol{E}^2_{t,TM} = & \sum_{m=0}^{\infty} \sum_{n=m}^{\infty} \left(\sigma^M_{mn} \boldsymbol{M}^{+(1)}_{o,m+1,n}(c_2) + \tau^M_{m+1,n+1} \boldsymbol{M}^{z(1)}_{o,m+1,n+1}(c_2) \right) \\ & + \sum_{n=1}^{\infty} \sigma^{M-}_{1n} \boldsymbol{M}^{-(1)}_{o1n}(c_2) \end{aligned} \tag{31b}$$

for the TE and TM polarizations, respectively. Note that the spheroidal radial functions of the first kind are now used instead because they are finite near the origin, and the transmitted wave has to be finite at the centre of the spheroid.

In the region $\xi_2 < \xi < \xi_1$, the transmitted waves are represented as

$$\begin{aligned} \boldsymbol{E}^1_{t,TE} = & \sum_{m=0}^{\infty} \sum_{n=m}^{\infty} \Big[\gamma^E_{mn} \boldsymbol{M}^{+(1)}_{e,m+1,n}(c_1) + \delta^E_{mn} \boldsymbol{M}^{z(1)}_{emn}(c_1) \\ & + \lambda^E_{mn} \boldsymbol{M}^{+(2)}_{e,m+1,n}(c_1) + \rho^E_{mn} \boldsymbol{M}^{z(2)}_{emn}(c_1) \Big], \end{aligned} \tag{32a}$$

$$\boldsymbol{E}^1_{t,TM} = \sum_{m=0}^{\infty} \sum_{n=m}^{\infty} \Big[\gamma^M_{mn} \boldsymbol{M}^{+(1)}_{o,m+1,n}(c_1) + \delta^M_{m+1,n+1} \boldsymbol{M}^{z(1)}_{o,m+1,n+1}(c_1)) \tag{32b}$$

$$+ \lambda_{mn}^{M} \boldsymbol{M}_{o,m+1,n}^{+(2)}(c_1) + \rho_{m+1,n+1}^{M} \boldsymbol{M}_{o,m+1,n+1}^{z(2)}(c_1)\Big]$$

$$+ \sum_{n=1}^{\infty} \Big[\gamma_{1n}^{M-} \boldsymbol{M}_{o1n}^{-(1)}(c_1) + \lambda_{1n}^{M-} \boldsymbol{M}_{o1n}^{-(2)}(c_1)\Big] \tag{32b}$$

for the TE and TM polarizations, respectively. γ_{mn}, $\delta_{m+1,n+1}$, λ_{mn} and $\rho_{m+1,n+1}$ are the unknown transmission coefficients to be determined. Note that in the coating region, both the first and the second kinds of spheroidal functions are used. This is because down over here, the wave consists of two components: one propagating inwards and one outwards.

Unlike the case of the perfectly conducting spheroid, the existence of fields inside the dielectric spheroid have to be considered, and the magnetic fields have to be considered in the boundary conditions. The magnetic fields in the different regions are related to the electric field via

$$\boldsymbol{H} = \frac{j}{kZ} \nabla \times \boldsymbol{E} \tag{33}$$

where k is the wave number and Z the characteristic impedance of the medium.

4.3 Transformation of Incident Fields to Scattered Fields

The boundary conditions satisfied by the electric and magnetic fields are

$$\xi = \xi_1 \ : \ E_\eta + E_{s\eta} = E_{t\eta}^1, E_\phi + E_{s\phi} = E_{t\phi}^1, \tag{34a}$$

$$\xi = \xi_1 \ : \ H_\eta + H_{s\eta} = H_{t\eta}^1, H_\phi + H_{s\phi} = H_{t\phi}^1, \tag{34b}$$

$$\xi = \xi_2 \ : \ E_{t\eta}^1 = E_{t\eta}^2 \quad E_{t\phi}^1 = E_{t\phi}^2, \tag{34c}$$

$$\xi = \xi_2 \ : \ H_{t\eta}^1 = H_{t\eta}^2 \quad H_{t\phi}^1 = H_{t\phi}^2. \tag{34d}$$

To obtain the transformation matrix, we use the same method as outlined previously for the conducting spheroid. Unlike that in the conducting case, the truncation number required to obtain a given accuracy in computing cross sections depends on a number of factors, for example, the electrical size, the material of the coating layer and the core spheroid, and the thickness of the coating layer. It is very difficult to come up with a rule that can take all these factors into account. As such, for the sizes and permittivities of the spheroids and their coatings

considered in this paper, we have found it sufficient to consider only $m = 0, 1, 2$ and $n = m, m+1, \cdots, , m+5$. The reason is that due to the dimensions of the matrices involved, it takes much longer time to compute the system for a given m, as compared to the conducting case. Moreover, the convergence has been verified by computing until $m = 4$ for most cases. In all instances, the results matched at least to four significant figures and in most cases to five significant figures. This ensures that the above scheme of truncation is proper.

5. RESULTS AND DISCUSSION

Some of the results obtained are shown here.

Fig. 3 illustrates the effect of the size of the spheroid on the backscattering cross section. The solid circles represent the results from Sinha and MacPhie [7] and Sinha and Sebak [16], and Sebak and Shafai [17]. As can be seen, the results from this paper are in very good agreement with the existing work. This verifies the accuracy of the *Mathematica* source codes developed. When $ka = 2$, the backscattering of both TE- and TM-mode waves shows a gradual increase in magnitude as the incident angle tends to 90° (where the surface area available for scattering becomes the maximum). As the spheroid becomes bigger with the increase in ka, the backscattering cross section becomes more oscillatory.

Fig. 4 shows the variation of the bistatic cross-sections for axial incidence ($\theta_0 = 0$) with two dielectric spheroids of the same axial ratios and permittivities but different semi-major axis lengths. The solid circles are the results from Asano and Yamamoto [10]. The close agreement once again verifies the accuracy of the *Mathematica* source code developed. For the smaller spheroid (top), the scattering intensity is almost a constant in the plane perpendicular to the plane of polarization of the incident wave (H-plane), whereas the scattering in the plane parallel to the plane of polarization (E-plane) is approximately proportional to $\cos^2\theta$. This is similar to the behaviour of the Rayleigh limit for the scattering by very small spheres, whose radii are much smaller compared to the incident wavelength. In such cases (the Rayleigh scattering), the intensity is a constant in the plane perpendicular to the plane of polarization, and varies as $\cos^2\theta$ in the parallel plane [18]. With the increase in size (bottom), the magnitude of the scattered intensity increases, and the forward scatter amplitude becomes much greater than the backscatter amplitude. Again, this

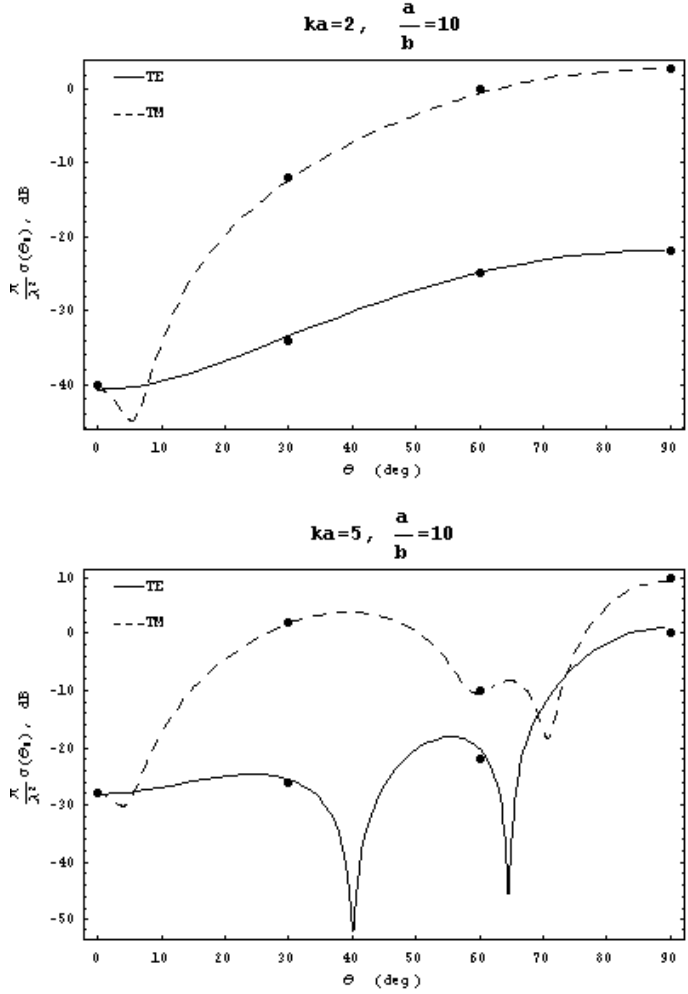

Figure 3. Backscattering cross-sections for perfectly conducting prolate spheroids with same axial ration 10, but different semi-major axial lengths.

is similar to the Mie effect observed in spheres [19]. In addition, the power patterns become more and more complicated, showing oscillating fluctuations with θ.

Fig. 5 illustrates two different backscattering cross sections of two coated spheroids of the same type of material but totally different dimensions. The one at the bottom has a much thicker coating relative to the inner core, and it is also fatter (with axial ratio of 2) than the

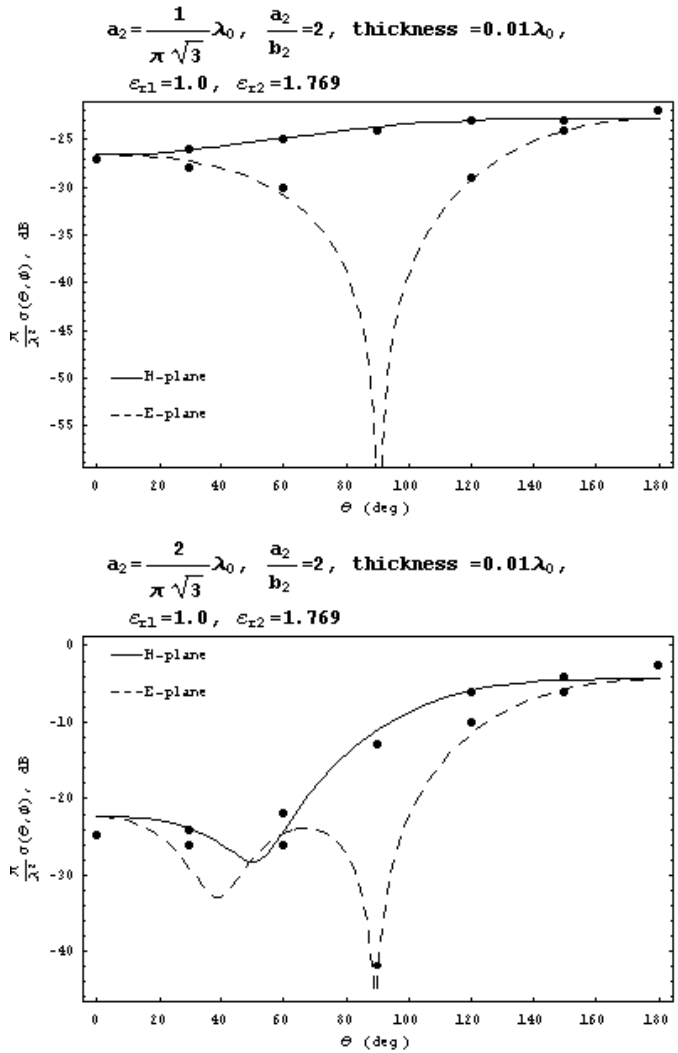

Figure 4. Bistatic cross-sections for dielectric spheroids at axial incidence with axial ratio 2, relative permittivity 1.769, but different sizes.

one at the top (with axial ratio of 5). The one with the thinner coating exhibits a TM backscatter that is always higher than the TE backscatter. For the one with the thicker coating, the TM backscatter starts off initially larger than the TE backscatter, but the TE backscatter increases steadily after $\theta_0 = 45^\circ$ until it is largest at broadside incidence ($\theta_0 = 90^\circ$).

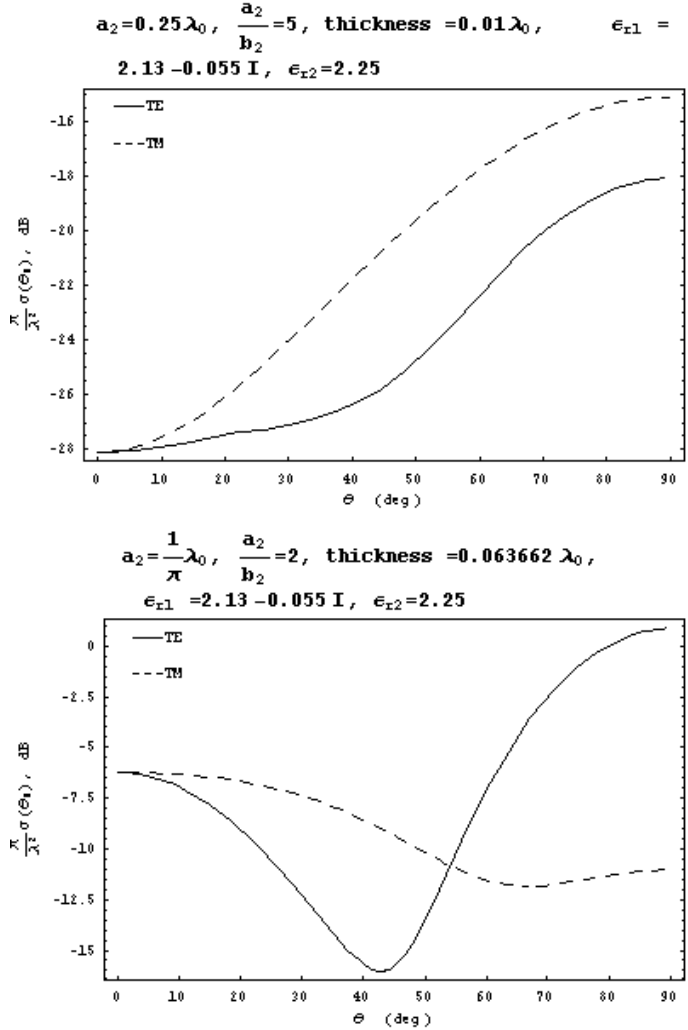

Figure 5. Backscatter cross-sections for coated dielectric spheroids with $\varepsilon_{r1} = 2.13 - 0.055i$, $\varepsilon_{r2} = 2.25$, but different dimensions and coating thicknesses.

Fig. 6 shows the variation of the bistatic cross sections with different angles of incidence for a dielectric spheroid with a confocal coating. For these cases, the plane of observation is taken to be the x-z plane. The shapes of the cross-sections remain about the same as the incident angle varies, but the minimum in the TM scattering moves towards the other end of the spheroid as the incident angle increases. The maximum

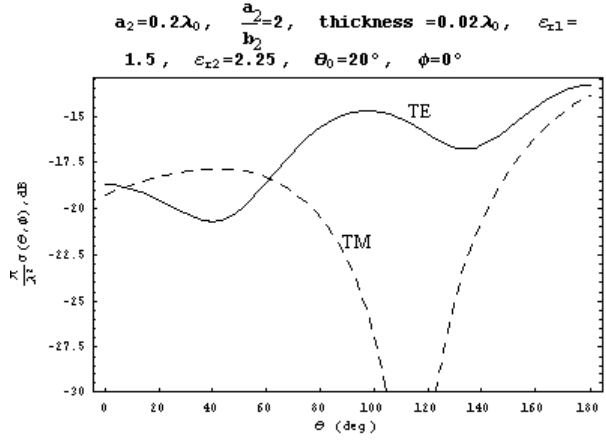
$a_2=0.2\lambda_0$, $\frac{a_2}{b_2}=2$, thickness $=0.02\lambda_0$, $\varepsilon_{r1}=$
1.5, $\varepsilon_{r2}=2.25$, $\theta_0=20°$, $\phi=0°$
TE
TM
$\frac{\pi}{\lambda^2}\sigma(\theta,\phi)$, dB
θ (deg)

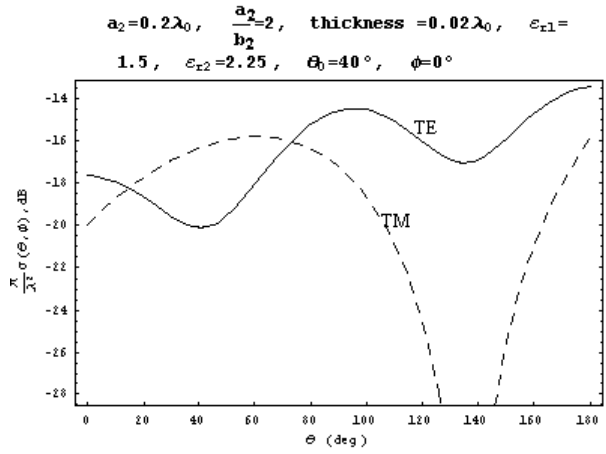
$a_2=0.2\lambda_0$, $\frac{a_2}{b_2}=2$, thickness $=0.02\lambda_0$, $\varepsilon_{r1}=$
1.5, $\varepsilon_{r2}=2.25$, $\theta_0=40°$, $\phi=0°$
TE
TM
$\frac{\pi}{\lambda^2}\sigma(\theta,\phi)$, dB
θ (deg)

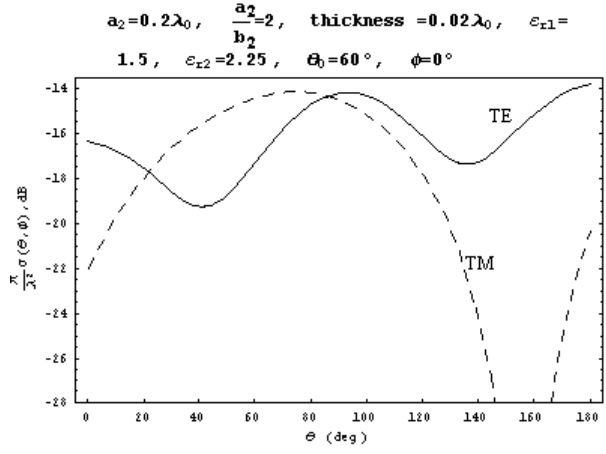
$a_2=0.2\lambda_0$, $\frac{a_2}{b_2}=2$, thickness $=0.02\lambda_0$, $\varepsilon_{r1}=$
1.5, $\varepsilon_{r2}=2.25$, $\theta_0=60°$, $\phi=0°$
TE
TM
$\frac{\pi}{\lambda^2}\sigma(\theta,\phi)$, dB
θ (deg)

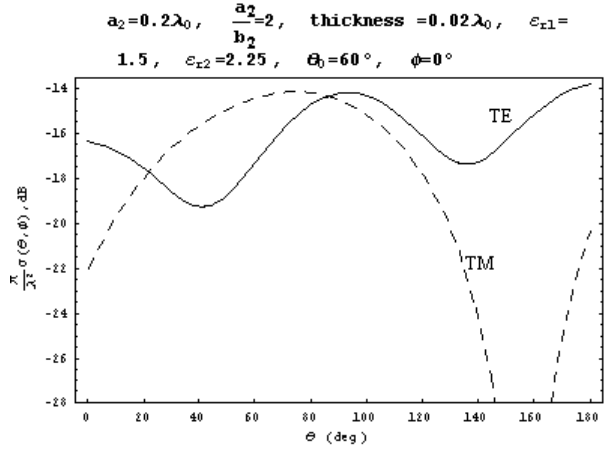

Figure 6. Bistatic cross-sections for a coated dielectric spheroid with $a_2 = 0.2\lambda_0$, axial ratio=2, coating thickness=$0.02\,\lambda_0$, $\varepsilon_{r1} = 1.5$ and $\varepsilon_{r2} = 2.25$, at angles of incidence, $20°$, $40°$, $60°$, and $80°$

in the TM scattering also increases, as the surface area available for scattering reaches the maximum at $\theta_0 = 90°$.

6. CONCLUSION

In this paper, the problem of electromagnetic scattering by a perfectly conducting spheroid and a coated dielectric spheroid is revisited and an exact solution to this problem has been obtained by using the method of separation of variables in the spheroidal coordinates system. The incident and scattered fields are expanded in terms of spheroidal vector wave functions and the expansion coefficients for the scattered wave are determined by an application of appropriate boundary conditions. Different from the previous work, this paper developed an accurate and efficient source code with Mathematica package for the numerical computations. So, the results obtained here are more accurate, as can be seen from the comparisons made in the paper. Also new to the existing work, bistatic and backscattering cross sections of a coated dielectric spheroid are computed and presented in this paper. It shows that the normalized bistatic and backscattering cross sections vary with the size and shape of the spheroid, as well as the type of material of the spheroid and the thickness and material of its coating in the case of the coated dielectric spheroid.

ACKNOWLEDGMENT

This work is supported in part by an ARF project grant PS990345 from the National University of Singapore and a SMA Fellow grant by Singapore-MIT Alliance (SMA) through High Performance Computation on Engineered System (HPCES) Programme.

REFERENCES

1. Stratton, J. A., *Electromagnetic Theory*, McGraw-Will, New York, 1941.
2. Van de Hulst, H. C., *Light Scattering by Small Particles*, John Wiley & Sons, New York, 1957.
3. Rheinstein, J., "Scattering of electromagnetic waves from dielectric coated conducting spheres," *IEEE Trans. Antennas Propagat.*, Vol. AP-12, No. 3, 334–340, March 1964.
4. Adey, A. W., "Scattering of electromagnetic waves by long cylinder," *Electron. Radio Eng.*, Vol. 35, 149–158, 1958.
5. Uslenghi, P. L. E., "High frequency scattering from a coated cylinder," *Canadian Journal of Physics*, Vol. 42, 2121–2128, 1964.
6. Siegel, K. M., F. V. Schultz, B. H. Gere, and F. B. Sleator, "The theory and numerical determination of the radar cross section of a prolate spheroid," *IRE Trans. Antennas Propagat.*, Vol. AP-4, 266–275, 1956.
7. Sinha, B. P. and R. H. MacPhie, "Electromagnetic scattering from prolate spheroids for axial incidence," *IEEE Trans. Antennas Propagat.*, Vol. AP-23, No. 5, 676–679, May 1975.
8. Sinha, B. P. and R. H. MacPhie, "Electromagnetic scattering by prolate spheroids for plane waves with arbitrary polarization and angle of incidence," *Radio Sci.*, Vol. 12, 171–184, 1977.
9. Flammer, C., *Spheroidal Wave Functions*, Stanford Univ. Press, California, 1957.
10. Asano, S. and G. Yamamoto, "Light scattering by a spheroidal particle," *Appl. Opt.*, Vol. 14, 29–49, 1975.
11. Cooray, M. F. R. and I. R. Ciric, "Scattering of electromagnetic waves by a coated dielectric spheroid," *J. Electromagn. Waves Applic.*, Vol. 6, 1491–1507, 1992.
12. Perterson, B. and S. Strom, "T-matrix formulation of electromagnetic scattering from multilayered scatterers," *Phys. Review D*, Vol. 10(8), 2670–2684, Oct. 1974.
13. Wang, D. S. and P. W. Barber, "Scattering by inhomogeneous nonspherical objects," *Appl. Opts.*, Vol. 18(8), 1190–1197, April

1979.

14. Li, L.-W., M.-S. Leong, T.-S. Yeo, P.-S. Kooi, and K. Y. Tan, "Computations of spheroidal harmonics with complex argument: A review with an algorithm," *Physical Review E*, Vol. 58, No. 5, 6792–6806, November 1998.
15. Stratton, J. A., P. M. Morse, L. J. Chu, J. D. C. Little, and F. J. Corbato, *Spheroidal Wave Functions*, John Wiley & Sons, New York, 1956.
16. Sinha, B. P. and A. R. Sebak, "Scattering by a conducting spheroidal object with dielectric coating at axial incidence," *IEEE Trans. Antennas Propagat.*, Vol. AP-40, No. 3, 268–274, 1992.
17. Sebak, A. and L. Shafai, "Electromagnetic scattering by spheroidal objects with impedance boundary conditions at axial incidence," *Radio Sci.*, Vol. 23, No. 6, 1048–1060, 1988.
18. Bohren, C. F. and D. R. Huffman, *Absorption and Scattering of Light by Small Particles*, John Wiley & Sons, New York, 1983.
19. Born, M. and E. Wolf, *Principles of Optics*, Pergamon Press, Oxford, 1970.